Development of a Converter-based Supercapacitor System Emulator for PV Applications

Paychuda Kritprajun
Department of Electrical Engineering and Computer Science
The University of Tennessee
Knoxville, TN, USA
pkritpra@vols.utk.edu

Elizabeth Sutton
Department of Electrical Engineering and Computer Science
The University of Tennessee
Knoxville, TN, USA
esutton4@utk.edu

Leon M. Tolbert
Department of Electrical Engineering and Computer Science
The University of Tennessee
Knoxville, TN, USA
tolbert@utk.edu

Yunting Liu
Department of Electrical Engineering
The Pennsylvania State University
University Park, PA, USA
ypl5778@psu.edu

Jingxin Wang
Department of Electrical Engineering and Computer Science
The University of Tennessee
Knoxville, TN, USA
jwang78@utk.edu

Nattapat Praisuwanna
Department of Electrical Engineering and Computer Science
The University of Tennessee
Knoxville, TN, USA
npraisu1@vols.utk.edu

Maximiliano Ferrari
Grid Components and Control
Oak Ridge National Laboratory
Oak Ridge, TN, USA
ferrarimagmf@ornl.gov

Abstract— As the utilization of supercapacitors in power system applications continues to increase, it is important to observe their behavior under transient and long-term operations in order to understand their impact on power grids. A real-time reconfigurable hardware testbed (HTB) is a power network emulator that provides flexibility to study various power system scenarios. This paper presents an emulation of a supercapacitor for a photovoltaic (PV) system on the HTB platform such that its dynamic behavior during power system scenarios can be observed. The developed emulator on the HTB is verified by comparing the emulation results with the model developed in MATLAB/Simulink. The experimental results of the emulator are consistent with the simulation results under the grid support scenarios. This supercapacitor emulator can be potentially used for various power system scenarios in addition to the PV applications presented in this paper.

Keywords—supercapacitor, grid-connected photovoltaic system, grid ancillary services, hardware testbed

I. INTRODUCTION

Supercapacitors (SCs) have gained more attention in power applications [1] due to their superior characteristics including high power density, ability to undergo numerous charge and discharge cycles, and long service life [1], [2]. For the power grid sector, SCs are normally used as short-term energy storage to smooth the power output from distributed energy resources such as wind and solar with intermittent behavior [3]. SCs are also used to provide ancillary services such as grid frequency regulation and inertia support [4], and voltage support [3].

It can be challenging to study the behavior of SCs in power systems using physical SCs, as it is difficult to maintain consistent testing conditions of the physical SC under numerous tests. SCs can be simulated in MATLAB/Simulink software using detailed models; however, the use of detailed models can be infeasible for large-scale power system analysis. Thus, a reconfigurable hardware testbed (HTB) has been developed to overcome the limitations of digital emulators and provide flexibility to study power systems at large-scale [5]. Multiple

voltage source converters (VSCs) in the HTB can be configured to emulate different grid components such as synchronous generators [6], energy storage (flywheel, battery [7], [8]), and static and dynamic loads ([9]–[11]) to perform multiple grid scenarios [5]. The emulators in the HTB can be reprogrammed and reconfigured, providing flexibility to represent different power system scenarios [5]. Despite the HTB's extensive capabilities, the HTB currently lacks an SC emulator, which limits the study of grid services offered by distributed energy storage resources that have been rapidly increasing in today's systems. Thus, this paper develops a SC emulator to fill a need of the SC energy storage technology for power system studies in the HTB platform.

In order to investigate SC dynamics under different power system test scenarios, the SC model should be selected so that it can accurately represent the short-term and long-term characteristics of the SC voltage [12], [13]. The series RC model is the simplest model since only two parameters are used to mimic the SC dynamics. However, it has a poor dynamic response when it comes to the long-term simulation [14]. Higher-order models such as Zubieta model, transmission model, and Stern model that can accurately represent the SC dynamics, both short-term and long-term might be a better fit. Considering the compromise between the model's complexity and its accuracy, the Zubieta SC model is considered a good candidate for power electronic grid interfaced applications [2], [13].

With the proper SC model and emulation development on the HTB platform, characteristics of SC for PV applications under various power system test scenarios can be observed. Since the system being emulated is a grid-connected PV with SC system (PVSS), the emulator will be referred to as PVSS for the rest of the paper. The PVSS emulator on the HTB is validated with the benchmark model developed in MATLAB/Simulink to ensure its accuracy under different tests. The developed emulator can be integrated into various types of power grid test scenarios addressing the study of future grids with more integrated SC systems.
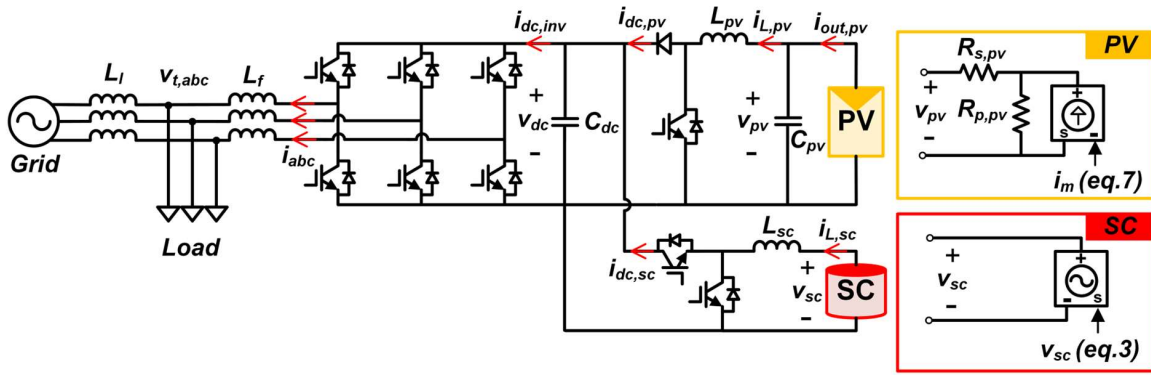
Fig. 1. Schematic of the grid-connected PV with SC system (PVSS).

The main contributions of this paper are as follows: 1) a PVSS emulator is developed on the HTB that can demonstrate the SC's dynamics for PV applications under power system scenarios; 2) digitized models of the developed emulator are derived and provided in detail; 3) common grid support functions are integrated in the emulator, which allows the SC's dynamics to be studied during grid support events.

II. EMULATOR SYSTEM AND CONTROL

The schematic of the grid-connected PV with SC system (PVSS) being emulated is shown in Fig. 1. The PVSS consists of a PV with its interface dc-dc boost converter, SC with its bidirectional dc-dc buck-boost converter, and a grid-connected inverter. The details of each system in the emulator are provided in the sections below.

A. Supercapacitor (SC) System

The Zubieta SC model is adopted in this paper as shown in Fig. 2. Each branch of the Zubieta's equivalent circuit model from the left to the right represents the SC response in seconds, minutes, longer than minutes, and leakage characteristic, respectively [12].

The internal parameters of the SC obtained from the experimental test are referred from [14], which represents the 3000F, 2.7 V SC manufactured by Maxwell (BCAP3000 [15]). The related parameters of the SC in the emulator are presented in Table I.
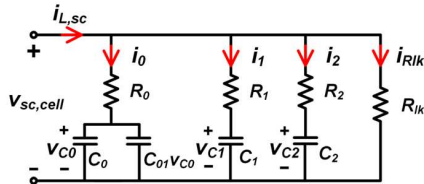

Fig. 2. The equivalent circuit of the Zubieta SC model [12], [14].

A bidirectional buck-boost dc-dc converter is used as an interface between the SC and the dc-link. The converter operates as a boost converter when discharging the SC, and as a buck converter when charging the SC [3]. An average current mode control, as presented in Fig. 3, is adopted to control the operation of the converter. This type of control is more stable than the voltage mode control and peak current mode control, thus it can ensure the stability of the converter with a wide range of operations during both buck and boost modes [3].

An outer PI control loop is used to control the dc-link voltage to its reference value, and this loop will generate the average current reference for the inner PI control loop. The SC dc-dc converter inductor current ($i_{L,sc}$) will be compared to the reference current to control the amount of the SC current during the operation, i.e., charging or discharging, in order to regulate the dc-link voltage to be close to its nominal value.

The PI compensators used in the SC's dc-dc converter are designed by using the transfer functions referred from [3]. The controller of the dc-link voltage control loop is designed to have lower bandwidth than the SC current loop's controller to be less sensitive to the noise [3]. The current control loop's controller is designed to have a high bandwidth with a faster response than the dc-link voltage control loop and enough phase margin to be stable. The controller's parameters of the SC's dc-dc converter based on the following design can be found in Table I.

Fig. 3. An average current mode control of the SC's dc-dc converter.

B. Photovoltaic (PV) System

The PV model adopted in this paper is obtained from [16]. This paper implements a double stage topology of the PV system, where the PV arrays connect to a dc-dc boost converter before connecting to the dc-link.

The PV system normally operates in maximum power point (MPP) mode to maximize its power generation. The MPP control based on the perturb and observe (P&O) method is adopted from [17]. The algorithm observes the PV powers before and after the change of the PV's system operation by adjusting the duty cycle of the PV's dc-dc converter. The new duty cycle will be determined to move the PV operation towards the maximum power by checking the changes in PV power and PV voltage based on the conditions described in Fig. 4.
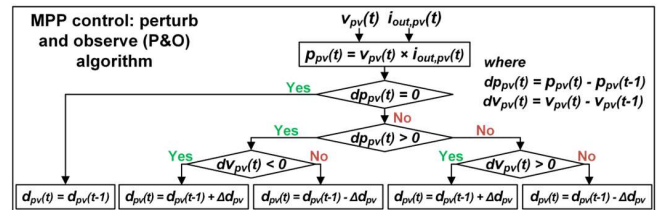

Fig. 4. MPP control of the PV's dc-dc converter [17].

C. Grid-connected Inverter

A grid-connected inverter is an interface connecting the dc-link to the rest of the power grid via an inductive filter (L_f). It controls the power flow between the power grid and the dc side (PV and SC systems) according to the PVSS operations.

This paper adopts a cascade inverter's control [18] in direct-quadrature (dq) coordinates shown in Fig. 5. The active power and reactive power (P_{inv}, Q_{inv}) are controlled by the outer PI controllers to follow their reference signals ($P_{inv,ref}, Q_{inv,ref}$). The inner loop is for controlling the inverter's currents (i_d, i_q) to track its reference currents ($i_{d,ref}, i_{q,ref}$) generated by the power control loops. After the compensation loops by the ac output frequency (ω) and the L_f, the duty cycle (d_{inv}) of the inverter is determined.

The controller parameters used in both control loops of the grid-connected inverter are provided in Table. I.
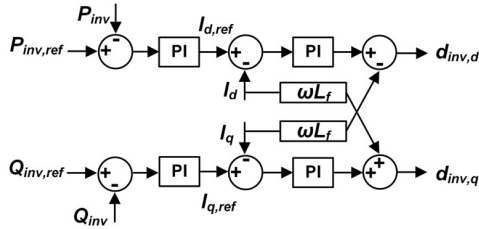

Fig. 5. Cascade control loop of the grid-connected inverter.

III. MODELING OF PVSS EMULATOR

A. Average Model of PVSS

This section presents the average model of each system in the PVSS. The parameters used in the equations in this section correspond to the labels in Fig. 1.

1) Average model of SC system

According to the SC model in Fig. 2, SC cell voltage ($v_{sc,cell}$) is calculated by using its relationship with the first branch capacitor charge (Q_0) [13] and its open circuit voltage ($v_{sc,ocv}$) as a function of its state of charge [19] as:

$$v_{sc,cell} = v_{sc,ocv} + R_0 i_0 + \frac{1}{C_{01}}\left(-C_0 + \sqrt{C_0^2 + 2C_{01}Q_0}\right) \quad (1)$$

Other SC parameters in (1), which correspond to their labels in Fig. 2 can be calculated as follows:

$$
\begin{aligned}
Q_0 &= \int i_0\, dt \\
i_0 &= \frac{i_{L,sc}}{N_{p,sc}} - i_1 - i_2 - i_{Rlk} \\
i_1 &= \frac{1}{R_1}(v_{sc,cell} - v_{c1}) \\
i_2 &= \frac{1}{R_2}(v_{sc,cell} - v_{c2}) \\
i_{Rlk} &= \frac{1}{R_{lk}}(v_{sc,cell}) \\
v_{c1} &= \frac{1}{C_1}\int i_1\, dt \\
v_{c2} &= \frac{1}{C_2}\int i_2\, dt
\end{aligned}
\quad (2)
$$

The sign of the $i_{L,sc}$ in (2) will change based on the SC operating conditions; $+i_{L,sc}$ when charging the SC and $-i_{L,sc}$ when discharging the SC.

SC cells are normally connected in series and/or parallel to form a SC module in order to meet the power, energy, and voltage based on the application's requirements. Voltage of the SC module (v_{sc}) can be calculated as:

$$v_{sc} = N_{s,sc} v_{sc,cell} \quad (3)$$

where $N_{s,sc}$ is the numbers of the SC cells connected in series and $N_{p,sc}$ is the numbers of the SC strings in parallel.

The state of charge of the SC module (SOC_{sc}) in percentage is represented by a ratio of the v_{sc} and the SC module rating voltage ($v_{sc,raing}$) as:

$$SOC_{sc} = \frac{v_{sc}}{v_{sc,raing}} \times 100 \quad (4)$$

The average model of the buck-boost dc-dc converter of the SC in continuous conduction mode (CCM) can be derived as:

$$
\begin{aligned}
L_{sc}\frac{di_{L,sc}}{dt} &= v_{sc} - v_{dc}(1 - d_{sc}) \\
i_{dc,sc} &= i_{L,sc}(1 - d_{sc})
\end{aligned}
\quad (5)
$$

where d_{sc} is the duty cycle of the SC's dc-dc converter.

2) Average model of PV system [16]

From the PV model developed by [16], the output current of the PV arrays ($i_{out,pv}$) can be derived as follows:

$$i_{out,pv} = \frac{R_{p,pv}}{R_{s,pv} + R_{p,pv}}\left(i_m - \frac{v_{pv}N_{p,pv}}{R_{p,pv}N_{s,pv}}\right) \quad (6)$$

where $N_{s,pv}$ is the number of series-connected modules per string and $N_{p,pv}$ is the number of parallel strings. The current source (i_m) of the PV model in (6) can be calculated as follows:

$$
\begin{aligned}
i_m &= i_{pv}N_{p,pv} - i_0 N_{p,pv}\left[\exp\left(\frac{v_{pv} + \frac{R_{s,pv}N_{s,pv}}{N_{p,pv}}i_{out,pv}}{v_{t,pv} \times a \times N_{s,pv}}\right) - 1\right] \\
i_{pv} &= \frac{G}{G_n}\left(I_{pvn} + K_i \Delta T_{pv}\right) \\
i_0 &= \frac{I_{pv,scn} + K_i \Delta T_{pv}}{\exp[v_{t,pv}(V_{pv,ocn} + K_v \Delta T_{pv}) - 1]} \\
v_{t,pv} &= \frac{k \times N_{s,cell} \times T_{pv}}{q} \\
\Delta T_{pv} &= T_{pv} - T_{pv,nom}
\end{aligned}
\quad (7)
$$

where i_{pv} is the light-generated current at the nominal condition. G is the irradiation in W/m² and T_{pv} is PV cell temperature in Kelvin. i_0 is the diode saturation current. $v_{t,pv}$ is the thermal voltage of $N_{s,cell}$ series-connected cells. This paper will not further discuss the PV model in detail. Additional information about the PV model can be found in [16], and the constants used in the equations are provided in Table I.

The input voltage of the PV's array (v_{pv}) in (6) is calculated by the average model of the PV's dc-dc converter in CCM as:

$$
\begin{aligned}
C_{pv}\frac{dv_{pv}}{dt} &= i_{out,pv} - i_{L,pv} \\
L_{pv}\frac{di_{L,pv}}{dt} &= v_{pv} - v_{dc}(1 - d_{pv}) \\
i_{dc,pv} &= i_{L,pv}(1 - d_{pv})
\end{aligned}
\quad (8)
$$

where d_{pv} is the duty cycle of the PV's dc-dc converter.

3) Average model of grid-connected inverter

An average model of a grid-connected inverter in the dq coordinate system is presented as follows:

$$L_f \frac{di_d}{dt} = v_{dc}d_{inv,d} - v_{t,d} + \omega L_f i_q$$
$$L_f \frac{di_q}{dt} = v_{dc}d_{inv,q} - v_{t,q} - \omega L_f i_d \tag{9}$$

The dc-link dynamic can be expressed by dc-link voltage (v_{dc}) and the summation of the currents from the dc-side systems ($i_{dc,pv}$, $i_{dc,sc}$) to the grid-side inverter ($i_{dc,inv}$). The dc-link voltage dynamic can be calculated as:

$$C_{dc} \frac{dv_{dc}}{dt} = i_{dc,pv} + i_{dc,sc} - i_{dc,inv} \tag{10}$$

where $i_{dc,inv}$ can be calculated by assuming the power entering the ac-side is equal to the power leaving the dc-side as mentioned in [8]. The power on the ac-side can be calculated by using the grid-side dq axis current (i_{dq}) and the voltage before the inverter filter ($v_{inv,dq}$), that can derive from (9). Below shows all related equations for calculating the $i_{dc,inv}$.

$$i_{dc,inv} = \frac{1.5}{v_{dc}} \left(v_{inv,d} i_d + v_{inv,q} i_q \right)$$
$$v_{inv,d} = v_{t,d} + L_f \frac{di_d}{dt} - \omega L_f i_q \tag{11}$$
$$v_{inv,q} = v_{t,q} + L_f \frac{di_q}{dt} + \omega L_f i_d$$

B. Discrete Model of PVSS

In order to emulate the PVSS on the HTB platform, each model in the system needs to be digitized in order to embed into an emulator's microprocessor [8], [10]. The HTB uses the digital signal processor (DSP) model TMS320F28335 from Texas Instruments as a microprocessor of the emulator. The sampling time (T_s) used in the discrete equations is based on the DSP sampling time at 0.1 ms.

The average models of the PVSS presented in Section III-A are converted to discrete formats by using the Forward Euler method, where the outputs of the computation cycle $[x + 1]$ are estimated by the results of the previous cycle $[x]$. The discretized model of the PVSS is presented in the sections below.

1) Discrete model of SC system

The Zubieta SC model in discrete format can be derived as:

$$v_{sc,cell}[x + 1] = v_{sc,ocv} + R_0 i_0[x]$$
$$+ \frac{1}{C_{01}} \left(-C_0 + \sqrt{C_0^2 + 2C_{01}Q_0[x]} \right) \tag{12}$$

Other SC parameters used in (12) can be calculated as:

$$Q_0[x + 1] = Q_0[x] + T_s i_0[x]$$
$$i_0[x + 1] = \frac{i_{L,sc}[x]}{N_{p,sc}} - i_1[x] - i_2[x] - \frac{v_{sc,cell}[x]}{R_{lk}}$$
$$i_1[x + 1] = \frac{1}{R_1} \left(v_{sc,cell}[x] - v_{c1}[x] \right)$$
$$i_2[x + 1] = \frac{1}{R_2} \left(v_{sc,cell}[x] - v_{c2}[x] \right) \tag{13}$$
$$v_{c1}[x + 1] = \frac{1}{C_1} \left(i_{1,int}[x] \right)$$
$$v_{c2}[x + 1] = \frac{1}{C_2} \left(i_{2,int}[x] \right)$$
$$i_{1,int}[x + 1] = i_{1,int}[x] + T_s i_1[x]$$
$$i_{2,int}[x + 1] = i_{2,int}[x] + T_s i_2[x]$$

$i_{1,int}[x]$ and $i_{2,int}[x]$ in the equations represent the integral of i_1 and i_2 over time, respectively.

The SC module's voltage can be calculated as:

$$v_{sc}[x + 1] = N_{s,sc} v_{sc,cell}[x + 1] \tag{14}$$

The discretized model of the buck-boost dc-dc converter of the SC can be derived as:

$$i_{L,sc}[x + 1] = \frac{T_s}{L_{sc}} \left(v_{sc}[x] - v_{dc}[x](1 - d_{sc}[x]) \right) + i_{L,sc}[x]$$
$$i_{dc,sc}[x + 1] = i_{L,sc}[x](1 - d_{sc}[x]) \tag{15}$$

2) Discrete model of PV system [16]:

The PV output current in the discrete format is:

$$i_{out,pv}[x + 1] = \frac{R_{p,pv}}{R_{s,pv} + R_{p,pv}} \left(i_m[x] - \frac{v_{pv}[x]N_{p,pv}}{R_{p,pv}N_{s,pv}} \right) \tag{16}$$

Other related parameters in (16) can be calculated as follows:

$$i_m[x + 1] = -i_0[x]N_{p,pv} \left[exp \left(\frac{v_{pv}[x] + \frac{R_{s,pv}N_{s,pv}}{N_{p,pv}} i_{out,pv}[x]}{v_{t,pv}[x] \times a \times N_{s,pv}} \right) - 1 \right]$$
$$+ i_{pv}[x]N_{p,pv}$$
$$i_{pv}[x + 1] = \frac{G[x]}{G_n} \left(I_{pvn} + K_i \Delta T_{pv}[x] \right) \tag{17}$$
$$i_0[x + 1] = \frac{I_{pv,scn} + K_i \Delta T_{pv}[x]}{exp \left[v_{t,pv}[x](V_{pv,ocn} + K_v \Delta T_{pv}[x]) - 1 \right]}$$
$$v_{t,pv}[x + 1] = \frac{k \times N_{s,cell} \times T_{pv}[x]}{q}$$
$$\Delta T_{pv}[x + 1] = T_{pv}[x] - T_{pv,nom}$$

The discrete model of the PV's dc-dc converter is derived as:

$$v_{pv}[x + 1] = \frac{T_s}{C_{pv}} \left(i_{out,pv}[x] - i_{L,pv}[x] \right) + v_{pv}[x]$$
$$i_{L,pv}[x + 1] = \frac{T_s}{L_{pv}} \left(v_{pv}[x] - v_{dc}[x](1 - d_{pv}[x]) \right) + i_{L,pv}[x]$$
$$i_{dc,pv}[x + 1] = i_{L,pv}[x](1 - d_{pv}[x]) \tag{18}$$

3) Discrete model of grid-connected inverter

The discrete model of the grid-connected inverter can be presented as:

$$i_d[x + 1] = \frac{T_s}{L_f} \left(v_{dc}[x]d_{inv,d}[x] - v_{t,d}[x] + \omega L_f i_q[x] \right) + i_d[x]$$
$$i_q[x + 1] = \frac{T_s}{L_f} \left(v_{dc}[x]d_{inv,q}[x] - v_{t,q}[x] - \omega L_f i_d[x] \right) + i_q[x] \tag{19}$$

The dc-link voltage dynamic in discrete format is:

$$v_{dc}[x + 1] = \frac{T_s}{C_{dc}} \left(i_{dc,pv}[x] + i_{dc,sc}[x] - i_{dc,inv}[x] \right) + v_{dc}[x] \tag{20}$$

The discrete format of the current from the dc side to the grid-side inverter ($i_{dc,inv}[x]$) can be calculated as follows:

$$i_{dc,inv}[x + 1] = \frac{1.5}{v_{dc}[x]} \left(v_{inv,d}[x]i_d[x] + v_{inv,q}[x]i_q[x] \right)$$
$$v_{inv,d}[x + 1] = v_{t,d}[x] + L_f \left(\frac{i_d[x+1] - i_d[x]}{T_s} \right) - \omega L_f i_q[x]$$
$$v_{inv,q}[x + 1] = v_{t,q}[x] + L_f \left(\frac{i_q[x+1] - i_q[x]}{T_s} \right) + \omega L_f i_d[x] \tag{21}$$

123

IV. Experimental Emulation of PVSS

A. Hardware Testbed Configuration

The PVSS emulator is implemented on the HTB by using three VSCs including generator emulator [6], load emulator [9], and PV combined with SC emulator as shown in Fig. 6. All emulators connect to each other through a line inductance (L_l) on the ac side to form the system under study. This enables the power flow between the emulators be similar to the power flow between grid components in the real power system.

Each emulator uses the real voltage and current measurements on the ac-side as inputs of the emulator's model, depending on the type of the emulator, i.e., voltage source or current source [20]. Since the PVSS is considered as a current source, then the VSC's terminal voltage ($v_{t,abc}$) will be measured and used as the input of the emulator. The abc/dq transformation embedded in the DSP calculates the voltage signals in dq coordinates for the synchronous frame phase-lock loop (PLL) to estimate the angle (θ) [10] that will be later used in the PVSS model.

The PVSS model will generate the dq current references depending on its operation mode based on the system condition received from the PLL block. The PVSS operating modes implemented in the emulator include a normal operation mode (MPP) and abnormal operation modes, where the PVSS will provide support to the grid i.e., voltage support, frequency support, and low-voltage ride-through (LVRT) operation. Then, the inner current control loop will use these reference currents to control the real VSC's current by generating the PWM signals. By doing it this way, the VSC can replicate the behavior of the PVSS without having physical connections to the real SC and PV systems.
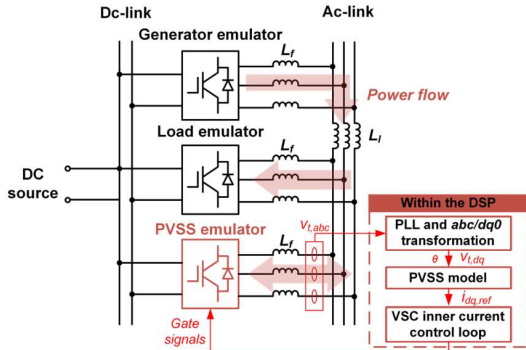
(a) The configuration of the PVSS on the HTB.
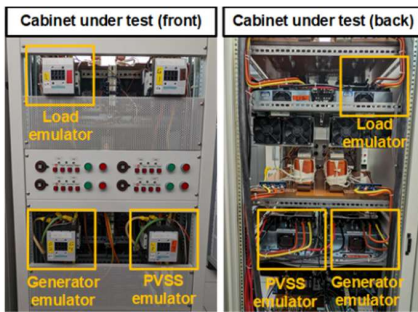
(b) Experimental test setup of the PVSS on the HTB.

Fig. 6.   Setup of the PVSS emulator on the HTB.

TABLE I.   PVSS'S EMULATOR PARAMTERS.

SC's Parameters	Values
Usable energy capacity	0.35 kWh
Usable power capacity	63.18 kW
Number in series ($N_{s,sc}$)	180
Number in parallel ($N_{p,sc}$)	1
Voltage rating ($v_{sc,raing}$)	486 V
Zubieta SC model [14]	R_0= 0.32232 mΩ, R_1= 0.38065 Ω, R_2= 1.3284 Ω, R_{lk}= 59.436 kΩ, C_0= 2934.7 F, C_{01}= 130.8 F, C_1= 76.841 F, C_2= 1518.8 F
Dc-dc converter rating	55 kW
Dc-dc converter's inductor (L_{sc})	0.4 mH
Dc-link voltage PI controller	$k_{p,v}$= 1.579 , $k_{i,v}$= 464.4
Current PI controller	$k_{p,i}$= 0.002396 , $k_{i,i}$= 8.557

PV's Parameters	Values
Power rating	50 kW
Number of series-connected modules per string ($N_{s,pv}$)	10
Number of parallel strings ($N_{p,pv}$)	17
Internal parameters of the PV's module: SunPower SPR-315E-WHT-D [21]	$R_{s,pv}$= 0.43 Ω, $R_{p,pv}$ = 430.07 Ω, G_n = 1000 W/m^2 , I_{pvn}= 6.1461A, $I_{pv,scn}$= 6.14 A, $V_{pv,ocv}$= 64.6 V, $N_{s,cell}$= 96, q = 1.6022e^{-19} C, a = 0.9507, k = 1.38062e^{-23} J/K, $T_{pv,nom}$ = 298.15 K, K_i= 0.061743 $\frac{\%}{^\circ C}$, K_v= -0.2727 $\frac{\%}{^\circ C}$
Dc-dc converter's inductor (L_{pv})	5 mH
Dc-dc converter's input capacitor (C_{pv})	100 μF

Dc-link's Parameters	Values
Voltage rating (v_{dc})	900 V
Dc-link capacitor (C_{dc})	1500 μF

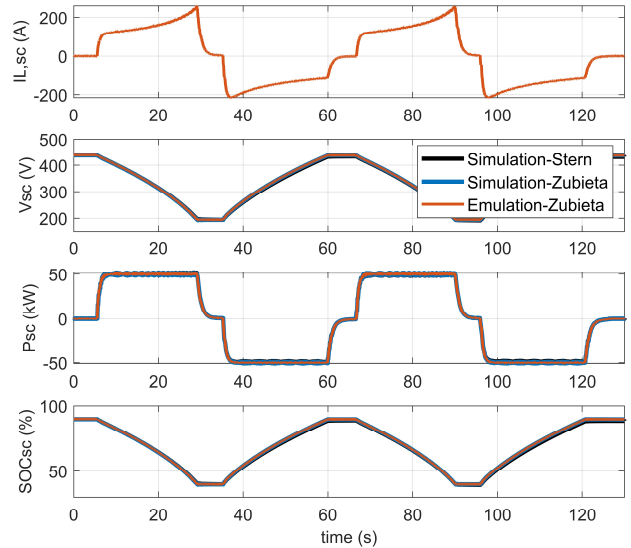| Inverter's Parameters	Values
Power rating	55 kW
Inductor filter (L_f)	0.5 mH
Line inductor (L_l)	2.3 mH
Outer loop active and reactive powers PI controllers	$k_{p,pq}$ = 2.871 , $k_{i,pq}$ = 57419
Inner loop currents PI controllers	$k_{p,i-dq}$ = 0.052 , $k_{i,i-dq}$ = 22.75

Fig. 7.   SC waveforms under constant power charge and discharge profiles.

124

B. Experimental Emulation Verification

The developed emulator on the HTB is verified by comparing the emulation results to the PVSS model developed in Simulink. The dynamics of the PVSS during the power system scenarios are demonstrated in the section below.

Grid support functions in terms of voltage and frequency regulation are implemented in the emulator so that the PVSS dynamics under these grid support events can be observed.

1) SC model verification

The accuracy of the Zubieta SC model adopted in the emulator is verified to represent the SC dynamic response with the models developed in the Simulink environment, including the Zubieta SC model and the SC Stern model [22] from the Simulink block.

As seen in Fig. 7, when the SC is being discharged or charged at a constant power (50 kW), the emulation results of the emulator closely follow the simulation results of the Zubieta model under the same charge and discharge profiles. However, the emulated SC voltage is slightly different over time when compared to the simulation results of the Stern model, since their models are different, yet their voltage patterns are similar.

2) Voltage support scenario

A grid voltage support scenario is conducted with the grid support function implemented in the emulator based on the reactive power-voltage (QV) droop curve from [23], [24].

The PVSS will provide reactive power support to the system when the grid voltage is out of its deadband, and the change of the reactive power reference during the support (ΔQ_v) can be calculated as follows:

$$\Delta Q_v = k_v \Delta v \tag{22}$$

where the coefficient of the voltage control loop (k_v) is 14.7 and Δv is the change in voltage during the disturbance compared to the deadband of the grid voltage.

Voltage scenarios have been performed with the results of both simulation and emulation shown in Fig. 8(a) undervoltage case and (b) overvoltage case, respectively. At the beginning of the events, the PVSS's voltage support function will be disabled and then later enabled to show the voltage improvement when the PVSS provides support to the system. In both voltage scenarios, the PV operates at 50 kW according to its rating before the voltage disturbances.

The voltage support of the PVSS is enabled at t = 17.4 s during the undervoltage of 0.91 pu; the PVSS provides reactive power at 0.44 pu of its rating while the SC absorbs PV power at 600 W to make room for reactive power support. The grid voltage increases to 0.94 pu during the support from the PVSS.

For the overvoltage scenario, the PVSS operation changes from injecting the reactive power to absorbing the reactive power from the grid in order to reduce the grid voltage. The grid voltage reduces from 1.08 pu to 1.06 during 0.44 pu of reactive power support from the PVSS.

The dynamics of simulation and emulation results for both voltage scenarios are consistent. However, the emulation results have a slower response time than the simulation due to the gradual change in the emulation's grid voltage. While the

emulation runs in real time, there is still some delays in measurement, control, and actuation [6]; thus, the emulation responses are more realistic than the results from the simulation.
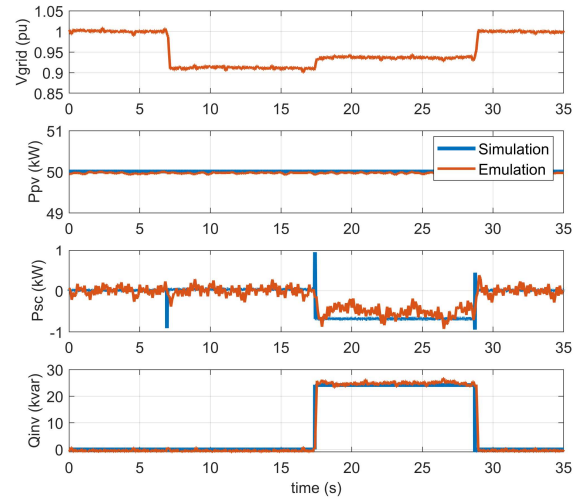
(a) undervoltage test scenario
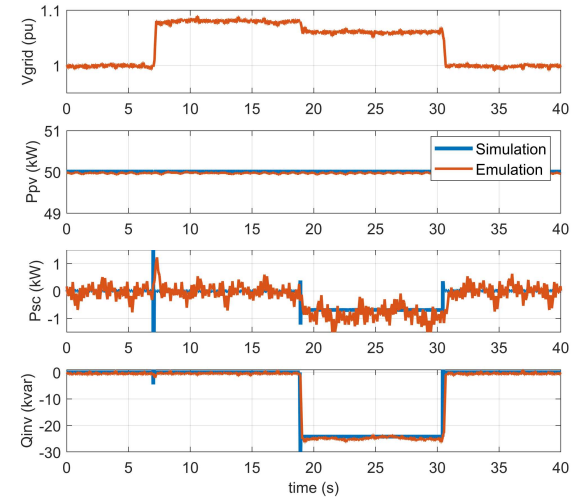
(b) overvoltage test scenario

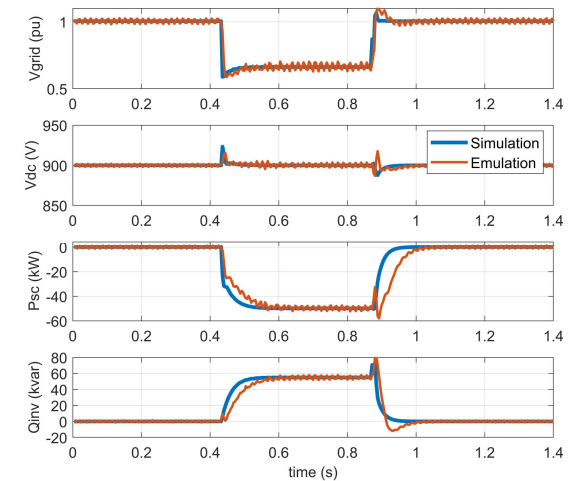Fig. 8. Grid voltage support scenarios.

Fig. 9. Low-voltage ride-through (LVRT) scenario.

125

3) Low-voltage ride-through (LVRT) scenario

The IEEE 1547 standard [23] requires the DER to stay connected to the grid and provide voltage support by adjusting its reactive power during voltage disturbances. Based on the IEEE 1547.9-2022 revision [25], the DERs with storage shall be able to provide LVRT services based on Category III, where the voltage of the mandatory operation is as low as 0.5 pu and the ride through time is up to 10 s.

During LVRT events, injecting the PV power generation to the grid can cause overcurrent in the inverter and overvoltage on the dc-link since the power cannot be injected to the grid. Thus, PV systems normally need to curtail their power in order to stay connected to the grid and provide support during LVRT events.

In order to emulate the low voltage condition for the LVRT scenario on the HTB as shown in Fig. 9, a step change of the load is applied to the system. The emulation voltage will drop to 0.58 pu during the LVRT scenario if the PVSS does not provide reactive power support to the system. For this scenario, the voltage support function in the PVSS emulator is revised to provide the full reactive power support at 55 kvar based on its power rating while the PV system operates at its maximum power of 50 kW.

At the beginning of the LVRT event when the grid voltage suddenly drops to a low value, the PVSS starts ramping up its reactive power to support the grid voltage while reducing its active power injected to the grid. The emulated powers have slower response time than the simulation due to some delays mentioned earlier, thus, their waveforms are slightly mismatch to the simulation. Meanwhile, the SC quickly absorbs the PV power at 50 kW in order to reduce the unbalanced power on the dc-link while the PV system continues its MPP operation during the event. The spikes of the dc-link voltage happen during the mode transitions between normal mode and LVRT operation, however, the dc-link voltage can be maintained at its nominal value quickly after the oscillations. The grid voltage can be improved to 0.67 pu during the reactive power support and the PVSS can remain connected to the grid complying with the standard's requirements during the LVRT operation.

4) Frequency support scenario

The PVSS adopts a fast frequency support function according to the standard IEEE1547.9-2022 revision [25] to provide both inertia support and frequency support to help the grid during frequency disturbances.

The PVSS needs to adjust its active power to slow down the rate of change of the frequency ($ROCOF$), simultaneously regulating the grid frequency as close to its nominal value as possible. The change in active power reference (ΔP_{fre}) during grid frequency support can be calculated as follows:

$$\Delta P_{fre} = k_{iner}ROCOF + k_f\Delta f \qquad (23)$$

where Δf is the change in frequency during the disturbance compared to the deadband of the grid frequency. The PVSS emulator adopts the moving average method to calculate the $ROCOF$ to avoid amplifying the noise of the frequency measurement when using the two-point method to calculate the $ROCOF$. The moving time window of the $ROCOF$ calculation is 0.5 s, which is in the range recommended by [26]. The coefficients of inertia control loop (k_{iner}) and frequency

control loop (k_f) are 2 and 0.5, respectively. The inertia and frequency support are activated based on each of their own deadbands at ±0.05 Hz/s and 36 mHz, respectively [23].

An under-frequency event is emulated by increasing the load as demonstrated in Fig. 10. The PVSS operates at 25 kW during this scenario; therefore, the active power support injected to the grid during the event will come from the SC.

The emulation results when the PVSS supports the grid are consistent with the results from the simulation as shown in Fig. 10(a). At the beginning of the frequency event, there is a sudden change in $ROCOF$; therefore, the SC immediately injects power to the grid to slow down the change of the frequency. Then, the SC continues injecting active power to increase the frequency to be close to its nominal value when the $ROCOF$ reduces close to zero.
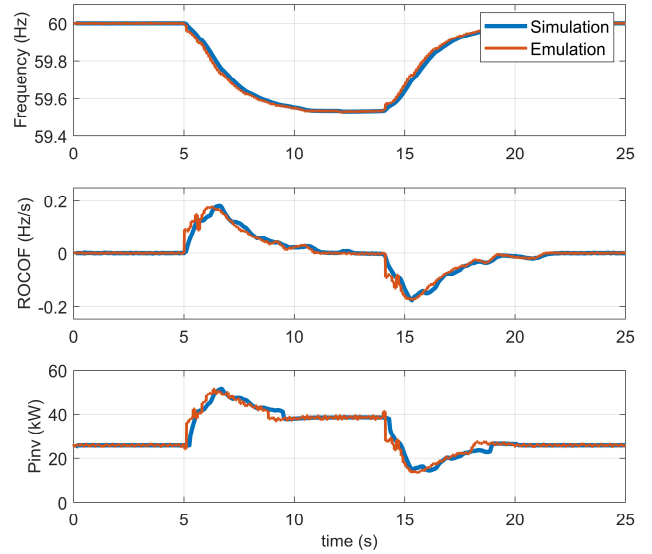
(a) Emulation and simulation results during under-frequency support scenario.
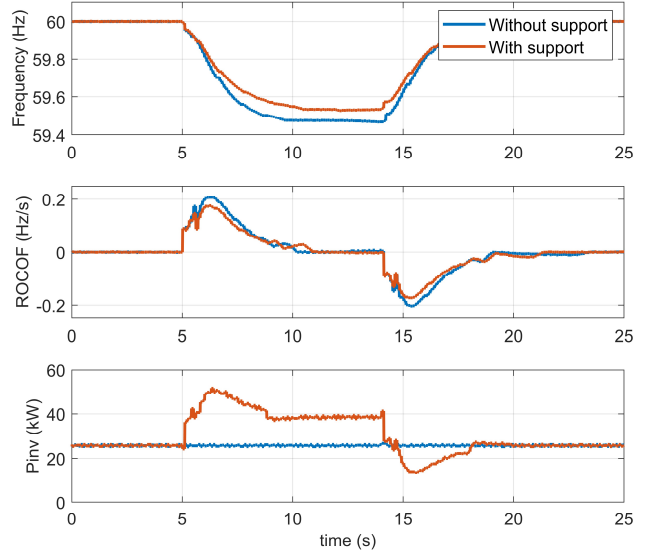
(b) Emulation results when providing the frequency support compared to the case without the frequency support.

Fig. 10. Grid under-frequency support scenario.

126

The performance of the frequency support provided by the PVSS based on the emulation is shown in Fig. 10(b). By comparing to the case when disabling the frequency support function, the PVSS can effectively provide fast frequency support to the grid by improving the grid frequency and reducing the *ROCOF* of the frequency event.

On the other hand, the PV system without energy storage cannot contribute to the under-frequency event since the PV power output mainly depends on the solar irradiation. Some PV systems might consider implementing PV headroom reserve control to account for the under-frequency support. However, the PV system will need to operate less than MPP, and it is not feasible during the nighttime with no solar irradiation.

Short-term energy storage can provide flexibility to operate the system while providing support to the grid. However, with its limited energy capacity, the design and operation will greatly impact service performance. Thus, the requirements of the grid support functions should be considered into the storage's sizing, charge management [27], and coordinated control with other systems such as PV curtailment control when the storage is unavailable.

V. Conclusions

To address an increased use of supercapacitors in power grids, a PVSS emulator is developed and demonstrated to accommodate the needs of power system tests related to grid-connected SC systems for PV applications. The Zubieta SC model is emulated on the HTB due to its compromise between complexity and accuracy. It can mimic the SC behavior accurately in both the short-term and long-term with moderate computation burden. Common grid support functions, in terms of voltage, frequency, and LVRT operation are implemented in the emulator to investigate the PVSS's dynamics during the grid support scenarios. The SC as an energy buffer of the PV system can effectively provide support during grid services due to its fast response. Thus, the PVSS can remain connected to the grid and provide support according to the grid's requirements. The developed emulator also provides flexibility to test various power system scenarios, as a single emulator or integrated with other emulators, such as PV, wind, and battery to represent a large-scale system.

References

[1] P. Roja, D. Venkatramanan and V. John, "A nonlinear model based analysis and accurate design of ultracapacitor stack for energy storage systems," in *IEEE Transactions on Energy Conversion*, vol. 37, no. 1, pp. 403-412, March 2022.

[2] M. E. Şahin and F. Blaabjerg, "A hybrid PV-Battery/Supercapacitor system and a basic active power control proposal in MATLAB/Simulink," in *Electronics*, vol. 9, no. 1, p. 129, Jan. 2020.

[3] D. Somayajula and M. L. Crow, "An ultracapacitor integrated power conditioner for intermittency smoothing and improving power quality of distribution grid," in *IEEE Transactions on Sustainable Energy*, vol. 5, no. 4, pp. 1145-1155, Oct. 2014.

[4] S. Karpana, E. Batzelis, S. Maiti, and C. Chakraborty, "PV-Supercapacitor cascaded topology for primary frequency responses and dynamic inertia emulation," *Energies*, vol. 14, no. 24, p. 8347, Dec. 2021.

[5] L. M. Tolbert et al., "Reconfigurable real-time power grid emulator for systems with high penetration of renewables," in *IEEE Open Access Journal of Power and Energy*, vol. 7, pp. 489-500, 2020.

[6] L. Yang et al., "Three-phase power converter-based real-time synchronous generator emulation," in *IEEE Transactions on Power Electronics*, vol. 32, no. 2, pp. 1651-1665, Feb. 2017.

[7] J. Wang, L. Yang, C. Blalock, and L. M. Tolbert, "Flywheel energy storage emulation using reconfigurable hardware test-bed of power converters," in *IEEE Electrical Energy Storage Applications and Technologies*, Oct. 2013, pp. 1–4.

[8] J. D. Boles, Y. Ma, J. Wang, D. Osipov, L. M. Tolbert and F. Wang, "Converter-based emulation of battery energy storage systems (BESS) for grid applications," in *IEEE Transactions on Industry Applications*, vol. 55, no. 4, pp. 4020-4032, July-Aug. 2019.

[9] J. Wang et al., "Static and dynamic power system load emulation in converter-based reconfigurable power grid emulator," in *IEEE Energy Conversion Congress and Exposition*, Pittsburgh, PA, USA, 2014.

[10] J. Sun, S. Wang, J. Wang and L. M. Tolbert, "Dynamic model and converter-based emulator of a data center power distribution system," in *IEEE Transactions on Power Electronics*, vol. 37, no. 7, pp. 8420-8432, July 2022.

[11] S. Wang, Y. Ma, J. Wang, L. M. Tolbert and F. Wang, "Variable speed drive connected motor load emulator for a multi-converter-based hardware testbed system," in *IEEE Open Journal of Industry Applications*, vol. 2, pp. 337-346, 2021.

[12] H. Miniguano, A. Barrado, C. Fernández, P. Zumel, and A. Lázaro, "A general parameter identification procedure used for the comparative study of supercapacitors models," in *Energies*, vol. 12, no. 9, May 2019.

[13] M. E. Şahin, F. Blaabjerg and A. Sangwongwanich, "Modelling of supercapacitors based on simplified equivalent circuit," in *CPSS Transactions on Power Electronics and Applications*, vol. 6, no. 1, pp. 31-39, March 2021.

[14] S. Pezzolato, "Modeling and model validation of supercapacitors for real-time simulations," M. S. thesis, University of Bologna, 2019.

[15] Maxwell Technologies, "2.7V 3000F ULTRACAPACITOR CELL," BCAP3000 P270 K04/05 datasheet, 2022. [Online]. Available: https://maxwell.com/wp-content/uploads/2022/11/3003279-EN.3_DS_2.7V-3000F-Cell-BCAP3000-P270.pdf

[16] M. G. Villalva, J. R. Gazoli and E. R. Filho, "Modeling and circuit-based simulation of photovoltaic arrays," in *Brazilian Power Electronics Conference*, Bonito-Mato Grosso do Sul, Brazil, 2009, pp. 1244-1254.

[17] Mathwork, "400-kW grid-connected PV farm (average model)," June 2023. [Online]. Available: https://www.mathworks.com/help/sps/ug/400-kw-grid-connected-pv-farm-average-model.html

[18] W. Wang, A. Beddard, M. Barnes and O. Marjanovic, "Analysis of active power control for VSC–HVDC," in *IEEE Transactions on Power Delivery*, vol. 29, no. 4, pp. 1978-1988, Aug. 2014.

[19] P. Saha, S. Dey, and M. Khanra, "Accurate estimation of state-of-charge of supercapacitor under uncertain leakage and open circuit voltage map," *Jounal of Power Sources*, vol. 434, 2019.

[20] Y. Ma, L. Yang, J. Wang, F. Wang and L. M. Tolbert, "Emulating full-converter wind turbine by a single converter in a multiple converter based emulation system," in *IEEE Applied Power Electronics Conference and Exposition*, Fort Worth, TX, USA, 2014, pp. 3042-3047.

[21] MathWorks, "Implement PV array modules," June 2023. [Online]. Available : https://www.mathworks.com/help/sps/powersys/ref/pvarray.html

[22] MathWorks, "Implement generic supercapacitor model," June 2023. [Online]. Available: https://www.mathworks.com/help/sps/powersys/ref/supercapacitor.html

[23] "IEEE Standard for Interconnection and Interoperability of Distributed Energy Resources with Associated Electric Power Systems Interfaces," in IEEE Std 1547-2018 (Revision of IEEE Std 1547-2003), pp.1-138, 6 April 2018.

[24] J. Giraldez, M. Emmanuel, A. Hoke and S. Suryanarayanan, "Impacts of Voltage-based Grid Support Functions on Energy Production of PV Customers," in *IEEE Power & Energy Society General Meeting*, Atlanta, GA, USA, 2019, pp. 1-5.

[25] "IEEE Guide for Using IEEE Std 1547 for Interconnection of Energy Storage Distributed Energy Resources with Electric Power Systems," in IEEE Std 1547.9-2022, pp.1-87, 5 Aug. 2022.

[26] NERC, "Fast Frequency Response Concepts and Bulk Power System Reliability Needs," June 2023. [Online]. Available: https://www.nerc.com/comm/PC/InverterBased Resource Performance Task Force.

[27] P. Kritprajun et al., "State of charge management for grid-connected PV with supercapacitor system considering LVRT operation," in *IEEE Energy Conversion Congress and Exposition*, Nashville, TN, USA, 2023.